Topologically protected Mach-Zehnder interferometer

Peilin Yang[1], Pengpeng Jiang[1], Xiaowei Guo[1, 2] and Lianping Hou[3]

[1] School of Optoelectronic Science and Engineering, University of Electronic science and Technology, Chengdu, China, 610054
[2] Center of Informational Biology, University of Electronic Science and Technology, Chengdu, China, 610054
[3] James Watt School of Engineering, University of Glasgow, Glasgow, G12 8QQ, UK

E-mail: gxw@uestc.edu.cn

Received xxxxxx
Accepted for publication xxxxxx
Published xxxxxx

Abstract

As photonic integration continues to evolve, compact and low loss Mach-Zehnder interferometer (MZI) has been an area of significant research inrecent years.Here, we propose a Valley-Hall effect based topologically protected Mach-Zehnder interferometer (TPMZI). Our simulations show that the TPMZI is efficient and stable even in complex situations. Sharp waveguide bending and defects such as obstructions and epitaxial , disorders, do not affect the propagation of photons along the interface, which guarantees the TPMZI high output power. In addition, the TPMZI yieldsexcellent sensitivity, extinction ratio and modulation depths, making it advantageous over existing systems when applied to optical communication, biochemical sensing, spectrometer analysis and measurementsystems, etc.

Keywords: topological photonics, interferometer, Valley Hall-Effect

1. Introduction

The Mach-Zehnder interferometer (MZI) detects phase variations between two light beams caused by a change of one of the paths, and is one of the most widely used structures in optical and photonic devices [1]. It has been utilized for realizing a variety of photonic devices such as optical switches, filters, modulators, sensors, amongt several other applications. With an ever-increasing demand for higher photonic integration with multiple components embedded on a sinlge chip, compact and low loss MZIs have been the subject of vast research efforts in recent years [2]. Conventional silicon MZI using standard waveguides is a relatively mature technology, but such MZIs have a fairly low propagation constant perturbation $\Delta\beta$. Because the phase change is related to the change of propagation constant and waveguide length L as $\Delta\phi = \Delta\beta \times L$, thus a large waveguide length is typically required. The length of interference arm in conventional silicon MZI usually requires several millimeters to meet the requirement of the phase shift [3-5]. Resonant enhancements can be employed to increase the sensitivity, however, can also limit the bandwidth of the device and make it prone to higher levels of fabrication imperfections and defects [6]. Unlike conventional silicon MZI, the photonic crystal (PC) based MZIs have a much larger $\Delta\beta$ by introducing slow-light effects. It can thus enable a substantial reduction ofthe length of the interference arm while preserving bandwidth, and in PC based MZIs, which is usually only a few tens of microns [7-9]. This not only makes the device more compact, but also promises low propagation loss and avoids the coupling losses at the input and output ports, as often seen in in conventional silicon MZI. Also to the detriment of existing MZIs with a design scheme realized by PCs, structural defects are highly probable in the fabrication

processes. As a result, backscattering loss of the photon stream is caused, resulting in power drop of the device. Therefore, fabrication imperfections will bring challenges to the reliability and yield of the devices.

In this paper, we solve this problem by introducing the concept of topologically protected MZI (TPMZI). Non-trivial topology provides the potential for unidirectional and lossless light propagation in optical devices [10-14]. Here we demonstrate that high output light transmittance and extinction ratio can be achieved by design without stringent geometrical requirements, and with a complete immunity to structural disorders, while retaining its interference ability.

2. Design of TPMZI

The TPMZI introduced here is schematically shown in Figure 1(a). It features a 2D hexagonal lattice of silicon rods embedded in the air background. The beam splitting and coupling are realized by the Y branch, which are separately denoted as *SP1* and *SP2*. To induce a non-trivial topology in TPMZI, we use valley photonic crystals (VPCs) to achieve topological phase transitions. The concept of VPCs was recently proposed by Ma etc. [11,13], which uses a valley degrees of freedom (DOF), similar to the binary spin DOF, to achieve the nontrivial topology by breaking the inversion symmetry. In this paper, we achieve this by tuning the radius of silicon rods [15,16], as shown in Figure 1(b). The parameter of δr defined by the difference in radius between two silicon rods is to describe the amplitude of inversion symmetry breaking [17]. We refer to the mode with $\delta r < 0a$ as VPC1 and $\delta r > 0a$ as VPC2. In Figure 1(c), a complete band gap from 0.266 to 0.302 *c/a* occurs when we set the radius of two silicon rods to $0.22a$ and $0.16a$ ($\delta r = 0.06a$), respectively. However, Berry phases for VPC1 and VPC2 are totally different [18]. When two VPCs contact each other, the local Chern number is not zero, which leads to a domain wall that supports the edge modes [19]. Due to different placement methods of two VPCs, there are two types of interfaces, namely 'S interface' and 'L interface', corresponding to the case VPC2 is on top of VPC1 and vice versa, respectively. Each interface ensures a wave propagation direction due to its essential immunity to backscattering [20,21]. To construct such TPMZI, a middle light channel is unavoidable between the reference and detection arms, as highlighted with a red box in Figure 1(a). On the other hand, according to the bulk-edge correspondence [22], a pair of edge state modes exist within the MZI band gap (see Figure 1(d)), denoting the 'S interface' and 'L interface' modes. To eliminate light propagation in the middle channel, a correct choice of the operating frequency range is necessary, promising a one-way propagation of the edge modes only in the reference and detection arms and thus MZI interference function remains unaffected.

We will verify the robustness of the MZI and its performance. The lattice constant is designed at a = 451nm. The electromagnetic wave in the TPMZI firstly enters a flat channel with a length of $36a$, and then is divided by the *SP1* that has a transition region with a length of $17a$. The splitting angles are both 120°, which is determined

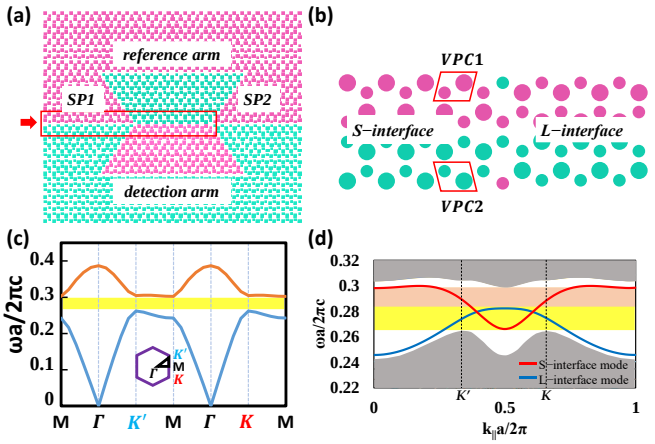

Figure 1. TPMZI structure with its bandgap and edge state modes. (a) Schematic of TPMZI. It consists of two types of interfaces and the enlarged view is shown in (b). We refer to the mode with $\delta r < 0a$ as VPC1 and $\delta r > 0a$ as VPC2. (c) The corresponding photonic band structures with broken inversion symmetry by tuning the radius of silicon rods. (d) Band diagrams of two topological edge states supported by the domain walls in (b).

by the VPCs arranged in a honeycomb lattice. After that, the electromagnetic waves pass through a flat path with a length of $34a$, and subsequently combine and interfere at the *SP2* terminal. In our design, the middle channel is constructed by the L-interface; therefore, we chose the operating frequency range from 0.282 *c/a* to 0.302 *c/a* which only contains S-interface mode, as the light-orange area highlights in Figure1(d). In the TPMZI, the so-called detection arm is filled with the sample to be measured and the reference arm with the air. When the refractive index of the surrounding material changes in the detection arm, the output intensity will change accordingly. The output transmittance of the TPMZI depends on the phase difference between the reference arm and the detection arm. If the effective refractive indices in the reference and detection arms are $\boldsymbol{n_{eff_1}}$ and $\boldsymbol{n_{eff_2}}$, then the phase difference between the arms of the interferometer is:

$$\boldsymbol{\Phi_d = \frac{2\pi}{\lambda} \cdot \left(n_{eff_1} \cdot l_1 - n_{eff_2} \cdot l_2\right)}, \qquad (1)$$

Where $\boldsymbol{l_1}$ and $\boldsymbol{l_2}$ are the lengths of the reference arm and the detection arm, respectively. The simulations in this paper were performed by a FDTD method, a TM linearly polarized Gaussian source is used and placed at the left entrance port, and the outer boundary condition is set to the perfect matching layer, which completely absorbs the incident electromagnetic waves and prevents electromagnetic wave reflections from propogating near the boundary. The VPC material is silicon, and the refractive indices were extracted from Palik's handbook [23].

3. Results and analysis

3.1 Broadband high transmission

In the case of no filler in the detection arm of VPCs, that is, the surrounding material is air, the optical path difference between the detection and reference arms is 0, leading to coherent interference at the output terminal. The transmittance of the TPMZI's *SP1* and *SP2* output terminals is presented in Figure 2(a). The frequency region of the edge states we chose to operate is shaded in light-orange rectangle and a broadband high transmission is achieved. As we can see, when the frequency of the edge states is located at the chosen region, the output transmission through TPMZI is almost the same as that of *SP1* output. This can be better understood by noticing that the frequency of the edge states located in the complete band gap region of silicon photonic graphene,so the scattering into bulk modes is forbidden. The backscattering between the forward and backward edge states is also blocked due to the suppression of inter-valley scattering. Therefore, broadband high transmission can be achieved. A Figure 2(b) to 2(d) showsthe electromagnetic waves with different frequencies that pass through the sharp bend waveguide without loss. This property is particularly interesting to develop efficient optical and photonic devices, for example, it is a good candidate for implementing photonic integrated circuits such as filters, wavelength demultiplexers or channel interleaves to be employed in high-speed Wavelength Division Multiplexing (WDM) [24].

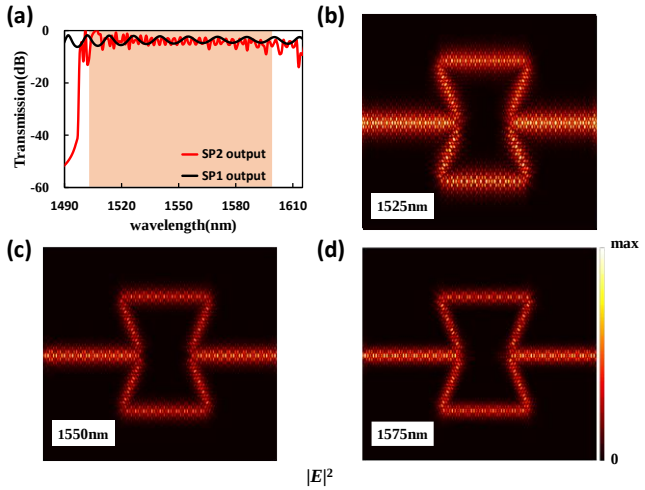

Figure 2. Broadband high transmission in TPMZI. (a) Transmissions of TPMZI. The black and red curves correspond to those at *SP1* and *SP2* output terminals, respectively. (b) - (d) The distribution of electric fields at (b) 1525nm, (c) 1550nm and (d) 1575nm.

3.2 Excellent sensitivity and high extinction ratio

We filled the sample to be measured in the detection arm, with the refractive index varied from 1 to 1.5 with a gradient interval of 0.05. The transmission output as a function of the refractive index at 1550 nm is shown in Figure 3(a). It can be seen that there are many cycles from 'on state' (constructive interference, see Figure 3(b)) to 'off state' (destructive interference, see Figure 3(c)) with the variation of the refractive index, which can be used for chemical and biological sensing purposes. For example, when the index varies from 1 to 1.15, it can be used for chemical gas detection and the sensitivity defined by the change of transmission divided by the change of index is 662%/RIU, which is sufficient to detect tiny changes of sample composition. However, when the index varies from 1.3 to 1.35, it can be utilized for detection of biological liquid samples. In addition, according to the extinction ratio formula:

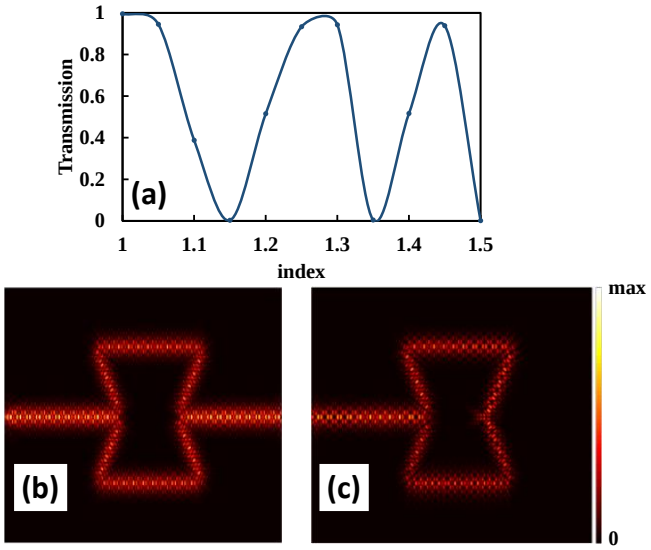

Figure 3. Extinction ratio and modulation depth of TPMZI at 1550nm. (a) Transmission output as a function of surrounding refractive index in TPMZI. (b) The distribution of electric fields when the refractive index in the detecting path is 1.0. The corresponding output power is 99.56%. (c) The distribution of electric fields when the refractive index in the detecting path is 1.15. The corresponding output power is 0.29%.

$$\boldsymbol{EXT = -10 \cdot lg(P_{off}/P_{on})}, \qquad (2)$$

We obtain that the extinction ratio is 25.3dB and the modulation depth is 99.3%. Table 1 presents a performance comparison of this TPMZI to other typical MZIs such as photonic crystal (PC) based and waveguide based MZIs. It can be seen that our proposed MZI has more compact size, high modulation depth and extinction, than other MZIs. Therefore, the TPMZI is very suitable as an optically controlled on-off switch or as an amplitude modulator.

Table 1 Comparison of typical MZI modulators

MZI type	Length of interference arm	Modulation depth	Extinction	Topological properties
TPMZI (this work)	15.3um	99%	25.3dB	Non-trivial
Waveguide based MZI [3]	3.45mm	84%	~12dB	trivial
Waveguide based MZI [8]	42um	~86%	14dB	trivial
PC based MZI [7]	80um	92%	20dB	trivial
PC based MZI [25]	250um	~93%	25dB	trivial

3.3 Defect immunity

Finally, we studied the wave propagation in a TPMZI that contains typical defects like obstruction and disorders, as shown in Figure 4(a) and 4(d). Such defects are created by adding a silicon rod in the detection arm and changing the radius of the interface rods due to imperfect fabrication where the diameter of upper row rods is increased by 3 nm and the lower row is reduced by 3 nm. In the obstruction case, due to the robust backscattering immunity of the interface mode, the wave propagation can flow round an obstruction and travel along the domain wall [see Figure 4(b)]. The transmission phase diagrams at the *SP2* end as a function of the refractive index within the detection arm is shown in Figure 4(c). It can be seen that in the presence of such defect, the phase at the *SP2* end exhibits slight change, which can be explained by the optical path being increased slightly because the topological edge states can bypass the defect without reflection. In the disorder case, the power in the detection arm is lower than that in the reference arm [see Figure 4(e)], which can be attributed to the fact that the propagation constant has changed and that of the reference arm is equivalent to that of the *SP1* channel. However, it is worth noting that in both cases, such defects are not the valley-mixing defects, thus the edge states along the domain wall will not be broken and the waves can still propagate without backscattering [see Figure 4(b) and 4(e)]. Such robust immunity against defects makes the TPMZI possible to realize unidirectional electromagnetic transport, even along a complex path, which greatly reduces the fabrication difficulties. This property is particularly interesting to optical biochemical sensing. For example, if some particles in sample solutions block the detection channel, we still achieve the sample information by using TPMZI structure. The robust immunity is also useful to develop high quality optical slow-light devices that are susceptible to backscattering [26].

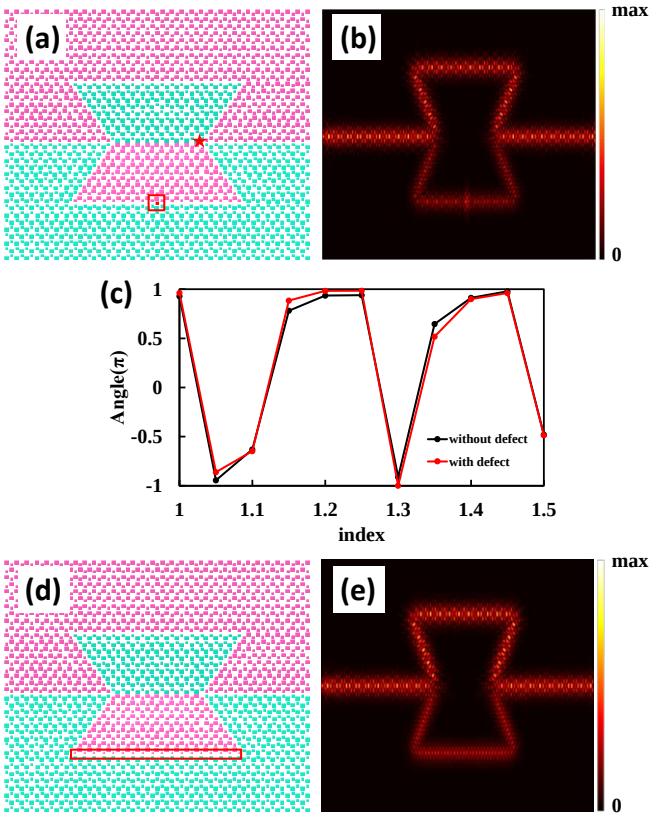

Figure 4. The robustness in TPMZI. (a) Schematic views of TPMZI that contains an obstructive defect. Star pattern marks the position of phase detection. (b) The corresponding electric field distribution of TMPZI at 1550nm. (c) The transmission phase diagrams at the *SP2* end in the two systems as a function of the refractive index within the detection arm of TMPZI. (d) Schematic views of TPMZI that contains a disordered defect in which diameters of two row rods are changed. (e) The corresponding electric field distribution of TMPZI at 1550nm.

4. Conclusion

In conclusion, we proposed a TPMZI based on the Valley-Hall effect. The proposed TPMZI exhibits high efficiency and stable characteristics. Defects such as sharp bending and

geometric defects will not affect the propagation of interface photons, resulting in high light transmittance and extinction ratio as well as high sensitivity. Since TPMZI has the property of defect immunity, it can be used as an efficient building block for many complex optical and photonic devices such as optical filters, wavelength demultiplexers, channels interleavers, intensity modulators, switches and optical gates, which may contribute to further advancements in optical communications, biochemical sensing, spectrometer analysis and optical measuring systems.

Acknowledgements

This work was supported by the Natural Science Foundation of Sichuan Province, China (Grant No. 2019YJ0172).

References

[1] Wo J H, Wang G H, Cui Y, Sun Q Z, Liang R B, Shum P P and Liu D 2012 Refractive Index Sensor Using Microfiber-based Mach-Zehnder Interferometer *Opt. Lett.* **37** 67

[2] Rizal C S and Niraula B 2018 Compact Si-based asymmetric MZI waveguide on SOI as a thermo-optical switch *Opt. Commun.* **410** 947

[3] Liao L, Samararubio D, Morse M and Liu A 2005 High speed silicon Mach-Zehnder modulator *Opt. Express.* **13** 3129-3135

[4] Zhao C Z, Li G Z, Liu E K, Gao Y and Liu X D 1995 Silicon on insulator Mach–Zehnder waveguide interferometers operating at 1.3μm *Appl. Phys. Lett.* **67** 2448-2449

[5] Schulz S A, O'Faolain L, Beggs D M and White T P 2010 Dispersion free slow light in photonic crystals: A comparison *J. Optics.* **12** 104004

[6] O'Faolain L, Beggs D M, White T P, Kampfrath T, Kuipers K and Krauss T F 2010 Compact Optical Switches and Modulators Based on Dispersion Engineered Photonic Crystals *IEEE. Photonics. Journal.* **2** 404-414

[7] Jiang Y Q, Wei J G, Gu L L, Chen X N and Chen R T 2005 80-micron interaction length silicon photonic crystal waveguide modulator *Appl. Phys. Lett.* **87** 221105

[8] Bakhshi S, Moravvej M K and Ebnali-Heidari M 2012 Design of ultra-compact low power all-optical Mach-Zehnder modulator by means of dispersion engineered slow light regime in photonic crystal *Nonlinear Optics and Applications VI* **8434** 843418

[9] Liu K, Zhang C, Mu S and Volker S 2016 Two-dimensional design and analysis of trench-coupler based Silicon Mach-Zehnder thermo-optic switch *Opt. Express* **24** 15845

[10] Hasan M Z and Kane C L 2010 Colloquium: Topological insulators *Rev. Mod. Phys.* **82** 3045

[11] Ma T and Shvets G 2016 All-Si valley-Hall photonic topological insulator *New. J. Phys.* **18** 025012

[12] Gao F, Xue H, Yang Z, Lai K, Yu Y, Lin X, Chong Y, Shvets G and Zhang B 2018 Topologically protected refraction of robust kink states in valley photonic crystals *Nat. Phys.* **14** 140

[13] Dong J W, Chen X D, Zhu H, Wang Y and Zhang X 2017 Valley photonic crystals for control of spin and topology *Nat. Mater.* **16** 298–302

[14] Nguyen B H, Zhuang X, Park H S and Rabczuk T, J. 2019 Tunable topological bandgaps and frequencies in a pre-stressed soft photonic crystal *Appl. Phys.* 125 095106

[15] Chen J J, Huo S Y and Zhu X F 2017 Topological valley transport of plate-mode waves in a homogenous thin plate with periodic stubbed surface *AIP. Adv.* **7** 115215

[16] Chen X D and Dong J W 2017 Valley-contrasting physics in all-dielectric photonic crystals: orbital angular momentum and topological propagation *Phys. Rev. B.* **96** 020202

[17] Chen X D and Dong J W 2016 Valley-protected backscattering suppression in silicon photonic graphene arXiv:1602.03352

[18] Xiao D, Yao W and Niu Q 2007 Valley-contrasting physics in graphene: magnetic moment and topological transport *Phys. Rev. Lett.* **99** 236809

[19] Khanikaev A B and Shvets G 2017 Two-dimensional topological photonics *Nature Photon.* **11** 763

[20] Mikael C R, Yaakov L and Segev M 2016 Topological Protection of Photonic Path Entanglement *Optica* **3**, 925

[21] Zhu H, Liu T W and Semperlotti F 2018 Design and experimental observation of valley-Hall edge states in diatomic-graphene-like elastic waveguides *Phys. Rev. B.* **97**, 174301

[22] Hatsugai Y 1993 Chern number and edge states in the integer quantum Hall effect *Phys. Rev. Lett.* **71** 3697

[23] Palik E D 1985 Handbook of optical constants of solids (Boston: Academic Press)

[24] Martínez A, Sanchis P and Martí J 2005 Mach–Zehnder interferometers in photonic crystals *Opt. Quant. Electron.* **37** 77-93

[25] Vlasov, Y A, O'Boyle M, Hamann H F, and Mcnab S J 2005 Active control of slow light on a chip with photonic crystal waveguides Nature **438** 65–69

[26] Povinelli M L, Johnson S G and E Lidorikis 2004 Effect of a photonic band gap on scattering from waveguide disorder *Appl. Phys. Lett.* **84** 3639